Journal of Neural Engineering

Modulation of neuronal activity and plasma membrane properties with low-power millimeter waves in organotypic cortical slices

To cite this article: Victor Pikov *et al* 2010 *J. Neural Eng.* **7** 045003

View the article online for updates and enhancements.

You may also like

- Millimeter-wave band optical single-sideband modulator using array-antenna-electrode and polarization-reversed structures with asymmetric Mach–Zehnder waveguide
Yuki Matsukawa, Toshiyuki Inoue, Hiroshi Murata et al.

- A high-accuracy calibration method for fusion systems of millimeter-wave radar and camera
Xiyue Wang, Xinsheng Wang and Zhiquan Zhou

- Multi-band passive detection and imaging system for concealed weapon with dual assessment method
Ahmet Ünal

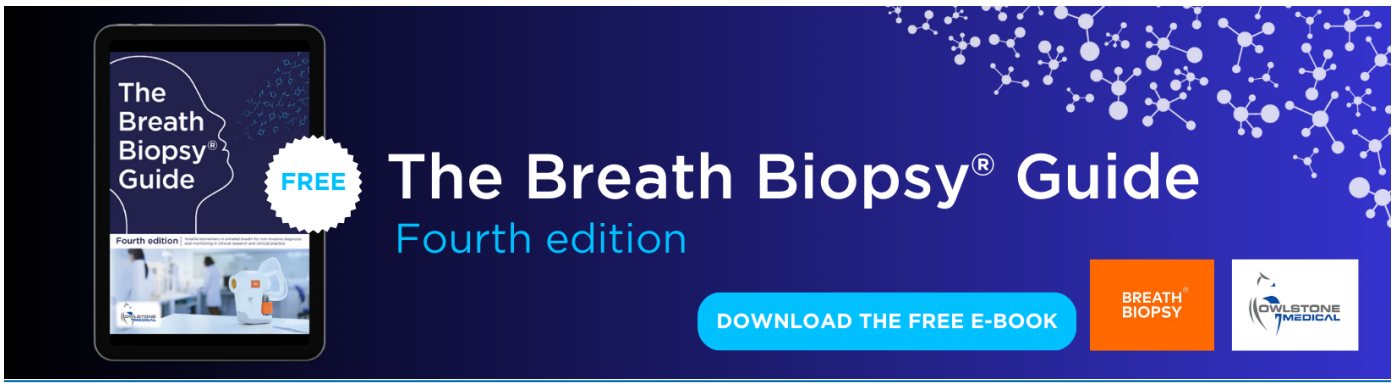

This content was downloaded from IP address 165.123.34.86 on 28/01/2024 at 19:10

J. Neural Eng. **7** (2010) 045003 (9pp) doi:10.1088/1741-2560/7/4/045003

Modulation of neuronal activity and plasma membrane properties with low-power millimeter waves in organotypic cortical slices

Victor Pikov[1,5], Xianghong Arakaki[2], Michael Harrington[2], Scott E Fraser[3] and Peter H Siegel[3,4]

[1] Neural Engineering Program, Huntington Medial Research Institutes, Pasadena, CA, USA
[2] Molecular Neurology Program, Huntington Medial Research Institutes, Pasadena, CA, USA
[3] Division of Biology, California Institute of Technology, Pasadena, CA, USA
[4] Division of Engineering and Applied Sciences, California Institute of Technology, Pasadena, CA, USA

E-mail: pikov@hotmail.com

Received 25 December 2009
Accepted for publication 30 April 2010
Published 19 July 2010
Online at stacks.iop.org/JNE/7/045003

Abstract
As millimeter waves (MMWs) are being increasingly used in communications and military applications, their potential effects on biological tissue has become an important issue for scientific inquiry. Specifically, several MMW effects on the whole-nerve activity were reported, but the underlying neuronal changes remain unexplored. This study used slices of cortical tissue to evaluate the MMW effects on individual pyramidal neurons under conditions mimicking their *in vivo* environment. The applied levels of MMW power are three orders of magnitude below the existing safe limit for human exposure of 1 mW cm^{-2}. Surprisingly, even at these low power levels, MMWs were able to produce considerable changes in neuronal firing rate and plasma membrane properties. At the power density approaching 1 μW cm^{-2}, 1 min of MMW exposure reduced the firing rate to one third of the pre-exposure level in four out of eight examined neurons. The width of the action potentials was narrowed by MMW exposure to 17% of the baseline value and the membrane input resistance decreased to 54% of the baseline value across all neurons. These effects were short lasting (2 min or less) and were accompanied by MMW-induced heating of the bath solution at 3 °C. Comparison of these results with previously published data on the effects of general bath heating of 10 °C indicated that MMW-induced effects cannot be fully attributed to heating and may involve specific MMW absorption by the tissue. Blocking of the intracellular Ca^{2+}-mediated signaling did not significantly alter the MMW-induced neuronal responses suggesting that MMWs interacted directly with the neuronal plasma membrane. The presented results constitute the first demonstration of direct real-time monitoring of the impact of MMWs on nervous tissue at a microscopic scale. Implication of these findings for the therapeutic modulation of neuronal excitability is discussed.

(Some figures in this article are in colour only in the electronic version)

[5] Author to whom any correspondence should be addressed.

 © 2010 IOP Publishing Ltd Printed in the UK

1. Introduction

Pervasive use of electromagnetic waves in modern society has strong potential implications for human health, and particularly for the activity of the nervous system. Widespread use of infrared waves and radiofrequencies (RF) in wireless communication has already stimulated an interest into their possible effects on the nervous tissue and led scientists to the discovery of considerable effects at 2 μm (150 THz) (Wells *et al* 2005a, 2005b) and 333 mm (900 MHz) (Hillert *et al* 2008, Wiholm *et al* 2009). Most recently, novel wireless video communication devices (Lawton 2008) and non-lethal military weapons (LeVine 2009) have been developed within the extremely high-frequency band of RF. This band spans 30–300 GHz, or wavelengths from 10 to 1 mm, and is formally designated as the millimeter wave (MMW) band. MMWs have low energy levels (0.12–1.2 meV) that are associated with molecular motion and intermolecular interactions, and are strongly absorbed by dipole-oriented molecules, such as water and phospholipids (Enders and Nimtz 1984, Liburdy and Magin 1985, Cametti *et al* 1988, Beneduci 2008, Ramundo-Orlando *et al* 2009). At 60 GHz, a commonly utilized MMW frequency, the absorption coefficient for water, tissue media and skin tissue ranges from 50 to 55 cm^{-1}, with almost all energy being absorbed within 0.4 mm (Zhadobov *et al* 2008). This strong absorption has been exploited for more than a half century for simple heating of biological tissue, but as the authors show in this paper, MMWs may also produce more subtle effects on the neuronal tissue at power levels well below the existing safe exposure limit of 1 mW cm^{-2} (Chou and D'Andrea 2005). Assuming that they show no long-term health impact, these effects might be exploited for regulating neuronal firing and, perhaps, other cellular activities.

The effects of MMWs on neural tissue have been previously examined only in whole-nerve preparations. In the first detailed study (Pakhomov *et al* 1997), MMWs (40–52 GHz) were applied to an isolated sciatic nerve in the frog. Using 20 min long exposures at the incident power density (IPD) of 2–3 mW cm^{-2}, a small increase (1–3%) in nerve firing was seen in several trials, while in others no changes were observed. In a more recent study by another group (Alekseev *et al* 2009), MMWs (42 GHz) were applied to the hind paw skin of an anesthetized mouse. During 1 min of MMW exposure to the skin area, firing of the sensory sural nerve was evaluated. At the IPD of 45–220 mW cm^{-2}, skin temperature was increased by 1.7–4.5 °C and strong (down to 44% of control) suppression of the nerve firing was observed. A radiant IR source, which resulted in equivalent skin heating of 4.5 °C, produced a similarly strong (40% of control) suppression of the nerve firing. In addition to the suppression of firing, the authors saw a transient (20–40 s) facilitation of the nerve firing, which was evident immediately after the MMW exposure, but not after the IR exposure. This capability of MMWs to produce opposite—excitatory and inhibitory—effects on the nerve activity is puzzling and warrants a more detailed evaluation of the MMW-induced neuronal effects with single-cell resolution. This study attempts to address this important question by using patch-clamp recording in a slice preparation of cortical tissue.

2. Methods

2.1. Animals and electrophysiological setup

Animal procedures were approved by the HMRI IACUC. Three neonatal P13–P16 Sprague-Dawley rats were deeply anesthetized by ketamine (87 mg kg^{-1}, IP) and xylazine (13 mg kg^{-1}, IP) and decapitated. The brains were removed and placed in a beaker for perfusion with ice-cold (0 °C) artificial cerebrospinal fluid (aCSF): a mixture of (in mM) 126 NaCl, 2.5 KCl, 2.4 $CaCl_2$, 1.3 $MgCl_2$, 1.2 NaH_2PO_4, 26 $NaHCO_3$ and 10 mM glucose (pH 7.4). The osmolarity of aCSF was 310–330 mOsm, as measured by depression of freezing point (Micro-Osmette, Precision Systems, Inc., Natick, MA). Slices (300 μm) containing the cerebral cortex were cut in the coronal plane with a motorized vibratome (World Precision Instruments, Sarasota, FL) and placed on a custom-made slice chamber for incubation at room temperature (20 °C) in an artificial cerebrospinal fluid solution (aCSF) (bubbled with 95% O_2, 5% CO_2, pH 7.4) for at least 1 h before patch clamp recording. All slices were used on the same day. For electrophysiological recording, the slice was placed in a tissue chamber (BT-1-18, Cell MicroControls, Norfolk, VA) and was continuously perfused with room-temperature aCSF using an inlet and outlet designed for turbulence-free laminar flow. The aCSF flow (1–2 ml min^{-1}) was controlled by gravity. Prior to MMW exposure, the amount of aCSF was minimized to allow better MMW penetration. Cortical layer 2/3 pyramidal neurons were visually identified under differential interference contrast (DIC) optics and IR illumination on an upright Nikon FN1 microscope with a 40× (0.8 N.A.) lens and a high-speed CCD camera (Qimaging). Glass recording electrodes (OD 1.5 mm, ID 1.12 mm, World Precision Instruments, Sarasota, FL) had a resistance of 4–7 MΩ when filled with a pipette solution containing (in mM) 140 K gluconate, 5 KCl, 4 NaCl, 10 HEPES, 0.3 Na_3GTP, 2 MgATP (pH 7.2–7.3, osmolarity 280–300 mOsm). For evaluation of the neuronal activity in the absence of intracellular calcium signaling, the intracellular calcium stores were buffered by adding 10 mM EGTA to the pipette solution. Whole-cell current-clamp recordings were obtained using a MultiClamp 700B patch amplifier, Digidata 1440 digitizer and a computer running pCLAMP software (all from Molecular Devices, Sunnyvale, CA). Data records were digitized at 10 kHz. The junction potential was around 10 mV, and all voltage recordings shown were not corrected for these potentials. Intracellularly injected current was held at 0 or negative values for 75% (15 s) of each 20 s cycle. Positive current (40–200 pA) was injected at 25% duty (5 s) during each cycle and the intracellular potential was recorded. Intracellular voltage measurements were analyzed in the beginning at 0.5 s after the initiation of current injection to avoid the initial variability in the AP firing rate. The action potential amplitude was defined as the difference between the pCLAMP-detected AP threshold and the positive peak. Time constants for rise and decay (τ_{rise} and τ_{decay}) of the action potential (AP) were calculated from the single-exponential functions, describing the full rising and decaying halves of the AP. These functions were derived from the data points by applying the Chebyshev

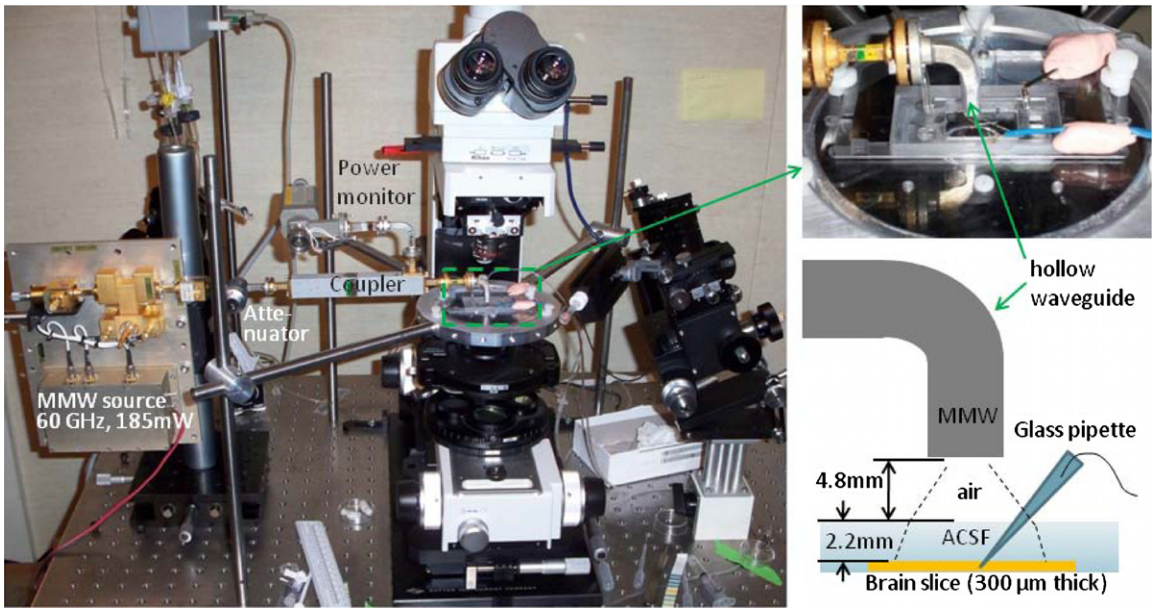

Figure 1. Left: electrophysiological setup with integrated MMW source. Right, top: close-up view of the tissue chamber and the hollow waveguide with an open-ended curved tip, allowing MMWs to be irradiated toward the tissue chamber. Right, bottom: schematic illustration of the MMW propagation from the tip of the waveguide. See the text for more details.

fitting algorithm. The apparent input resistance was calculated by dividing the change in the resting membrane potential by the amplitude of the injected depolarizing current: $R_n = \Delta V/\Delta I$.

2.2. MMW exposure

The MMW exposure system (figure 1) consisted of a custom-assembled MMW source (injection-locked IMPATT oscillator) operating at 60.125 GHz and producing up to 185 mW of continuous wave power at the exit of the open-ended WR-15 waveguide. Power was continually monitored through a directional coupler and calibrated RF power meter (HP 436A, Agilent Technologies, Santa Clara, CA). The power emitting on the tissue chamber was controlled by a rotary vane attenuator that could reduce the power to below detectable level ($<1\ \mu$W) without throwing an electrical switching discharge. The rectangular waveguide with 3.8×1.9 mm^2 aperture was carefully positioned above the tissue chamber, blocking the path of the microscope. The MMW power was directed perpendicular to the plane of the chamber for more uniform irradiation of the area occupied by the tissue slice. The tip of the waveguide was placed just beyond the far field distance of the tissue with an air gap of 4.8 mm to the surface of the aCSF solution and approximately 7 mm to the top of the slice. The linearly polarized RF fields exiting the rectangular waveguide expand at a half angle of $\sim 27^\circ$ in the H plane (parallel to the wide wall) and 56° in the E plane (along the short wall) creating a half-power ellipse of 5.5 mm^2 (major and minor axes of 14.2 and 4.9 mm, respectively) at the aCSF surface. The RF beam is refracted upon entering the solution and forms a half-power ellipse of 6.5 mm^2 (major and minor axes of 15.2 and 5.4 mm, respectively) at the top of the slice, 2.2 mm below the aCSF surface. A large portion of the incident RF signal is reflected upon contact with the fluid surface and is assumed to be radiated into the surrounding space without absorption by the fluid. Using published data for the complex permittivity of water and water-based media at 60 GHz (Zhadobov *et al* 2008), we calculated the reflected power to be $\sim$45%, leaving 55% of the available power for absorption by aCSF. Using the published data for the same frequency and similar ionic media (Zhadobov *et al* 2008) and Beer's law ($I = I_0\,\mathrm{e}^{-\mathrm{a}x}$) for the intensity drop with penetration depth x (in cm), we estimated the loss tangent for MMW absorption by aCSF to be 1.48. This translates into the absorption coefficient of 52 cm^{-1}, indicating the power drop of 99.5% by 1 mm of aCSF. Using a further approximation that the energy in the RF beam is uniformly distributed over the tissue within the half-power ellipse, the maximal power of 185 mW exiting the waveguide port produces a power density of approximately 90 mW cm^{-2} transmitted into the aCSF and less than 1 μW cm^{-2} at the tissue level, 2.2 mm below the surface. Therefore, in this study, the highest applied IPD of MMWs at the level of slice neurons is 1000 times lower than the most conservative current safe exposure level of 1 mW cm^{-2} (Chou and D'Andrea 2005).

During MMW exposure, the aCSF temperature containing the cortical slice was monitored using a thermocouple probe positioned near the bottom of the well 3 cm away from the center of the chamber. The probe was connected to a TC2BIP temperature controller with 0.1 °C accuracy and digital readout screen (Cell MicroControls, Norfolk, VA). To compensate for the delay in horizontal heating transfer from the center to the periphery of the chamber, thermal recordings were calibrated with a probe positioned at the depth of 2.2 mm either directly under the waveguide or 3 cm away from the waveguide. The applied corrections for different IPDs were +0.1 °C for 280 nW cm^{-2}, +0.3 °C for 560 nW cm^{-2} and +0.5 °C for 840 nW cm^{-2}.

Table 1. Analysis of the AP-related and membrane parameters in two subsets of cortical neurons. Statistical significance (p) indicates difference from the pre-exposure control, based on the Dunnett *post hoc* test, and is marked as follows: <0.05 (*), <0.01 (**).

Neuronal group	Parameter	Pre-MMW exposure	During MMW exposure at following IDP ranges (nW cm^{-2})					
			30–50	70–90	140–200	250–330	490–600	700–800
#1 ($n = 4$)	AP amp. (mV)	72 ± 2	73 ± 1	74 ± 2	75 ± 2	76 ± 4	76 ± 5	82 ± 5*
	Firing rate (Hz)	3.2 ± 0.2	2.8 ± 0.3	3.2 ± 0.3	3.1 ± 0.4	2.0 ± 0.6	0.9 ± 0.2*	1.3 ± 0.4*
	τ_{rise} (ms)	0.73 ± 0.15	0.63 ± 0.1	0.51 ± 0.06	0.56 ± 0.08	0.4 ± 0.06	0.28 ± 0.06*	0.25 ± 0.06*
	τ_{decay} (ms)	9.7 ± 1.7	8.8 ± 3.7	7.9 ± 2.0	6.5 ± 1.9	3.8 ± 1.1	2.6 ± 0.9*	1.0 ± 1.1**
	R_n (MΩ)	308 ± 69	397 ± 56	287 ± 77	283 ± 54	229 ± 45	148 ± 18*	173 ± 34*
#2 ($n = 4$)	AP amp. (mV)	42 ± 4	41 ± 5	43 ± 6	45 ± 5	52 ± 6	50 ± 8	45 ± 13
	Firing rate (Hz)	5.6 ± 0.3	5.9 ± 0.1	6.0 ± 0.3	6.4 ± 0.4	7.1 ± 0.5	8.1 ± 1.1*	6.5 ± 0.5
	τ_{rise} (ms)	1.1 ± 0.15	1.07 ± 0.18	0.98 ± 0.14	0.92 ± 0.15	0.55 ± 0.09	0.42 ± 0.05**	0.36 ± 0.18*
	τ_{decay} (ms)	5.1 ± 0.5	5.5 ± 0.9	5.1 ± 0.7	4.5 ± 0.9	3.2 ± 0.7	2.3 ± 0.7*	1.1 ± 0.6**
	R_n (MΩ)	423 ± 42	448 ± 56	394 ± 38	372 ± 41	274 ± 29	243 ± 34*	208 ± 86*

Table 2. Analysis of the AP-related and membrane parameters of cortical neurons during MMW exposure and bath heating. Statistical significance (p) indicates difference from the pre-exposure control, based on the Dunnett *post hoc* test, and is marked as follows: <0.05 (*), <0.01 (**).

Parameter	Pre-MMW exposure	During exposure at 490–600 nW (cm^{-2})	During exposure at 700–800 nW (cm^{-2})	Pre-bath heating[a]	During bath heating[a]
Bath T (°C)	20.0	22.1	23.2	23	33
AP amp. (mV)	57 ± 6	61 ± 7	57 ± 12	90 ± 11	76 ± 8
Firing rate (Hz)	4.4 ± 0.5	5.0 ± 1.6	4.8 ± 1.8	N.A.	N.A.
τ_{rise} (ms)	0.92 ± 0.12	0.36 ± 0.04**	0.33 ± 0.11*	0.90 ± 0.27	0.51 ± 0.13*
τ_{decay} (ms)	7.4 ± 1.2	2.4 ± 0.5**	1.1 ± 0.3**	2.8 ± 1.1	1.7 ± 0.4*
R_n (MΩ)	366 ± 43	202 ± 27**	196 ± 51*	389 ± 151	254 ± 96*

[a] The neuronal parameters from a published report (Lee *et al* 2005), where bath heating was produced by an in-line water heater.

We used general linear model (GLM) followed by the Dunnett *post hoc* test on predefined comparisons against the pre-exposure control using the Minitab software (Minitab Inc., State College, PA). Significance was set at $p < 0.05$ (*) and $p < 0.01$ (**). The values in tables 1 and 2, and figure 3 are expressed as mean ± standard deviation.

3. Results

Whole-cell recordings were made in freshly prepared slices of the cerebral cortex of neonatal rats. Neurons of pyramidal phenotype located in the layer 2/3 of the cortex were selected using infrared videomicroscopy with DIC enhancement. A total of eight neurons were patched in eight slices from three rats. After the neurons were patched and their microscopic visualization was no longer necessary, the MMW exposure system was moved into place and used to illuminate the tissue chamber with a series of IPDs in random order. Prior to the MMW exposure, the fluid flow through the chamber was halted and aCSF was partially removed from the well containing the tissue slice until visual confirmation of a concave meniscus formed at the fluid surface. The remaining amount of aCSF in the chamber was 0.9–1.1 ml and the depth of solution covering the slice was between 2.1 and 2.3 mm. This depth was sufficient to fully stabilize the temperature in the fluid above the slice and allow sufficient nutrition to the neurons during the measurement sequence lasting 25–30 min. A thermal sensor was located close to the slice, assuring that the slice was exposed to an equivalent amount of aCSF-damped heating from the MMW source. The actual power, generated by the MMW source, was measured throughout the experiment using an inline directional coupler and the calibrated power meter (figure 1).

In order to improve neuronal viability and stability of the neuronal firing in the whole-cell recordings, the depolarizing current was injected intracellularly at a 25% duty cycle (figure 2). Several MMW power levels were applied to the slice in randomized order to remove any possible effects of cumulative exposure. Each exposure lasted for 60 s (or three 20 s cycles); thus, three 5 s neuronal activity records were collected during the exposure. In a presented example (figure 2), exposure of the neuron n14 with a low MMW IPD of 71 nW cm^{-2} produced no significant effect on the neuronal firing rate during the exposure and a small increase in firing rate after the exposure. Higher IPD levels (from 284 to 737 nW cm^{-2}) produced considerable suppression of neuronal firing during the exposure and strong facilitation of firing immediately after the exposure.

Next, we examined the latency of neuronal responses to MMWs. We evaluated the changes in the membrane input resistance R_n, estimated as the change of the resting membrane potential during the injection of depolarizing current ($\Delta V/\Delta I$). This parameter was not dependent on the presence of the APs and thus, was not susceptible to confounding variability in the AP firing rate. An averaged R_n value was calculated for each 5 s period of current injection in 20 s intervals. The IPD

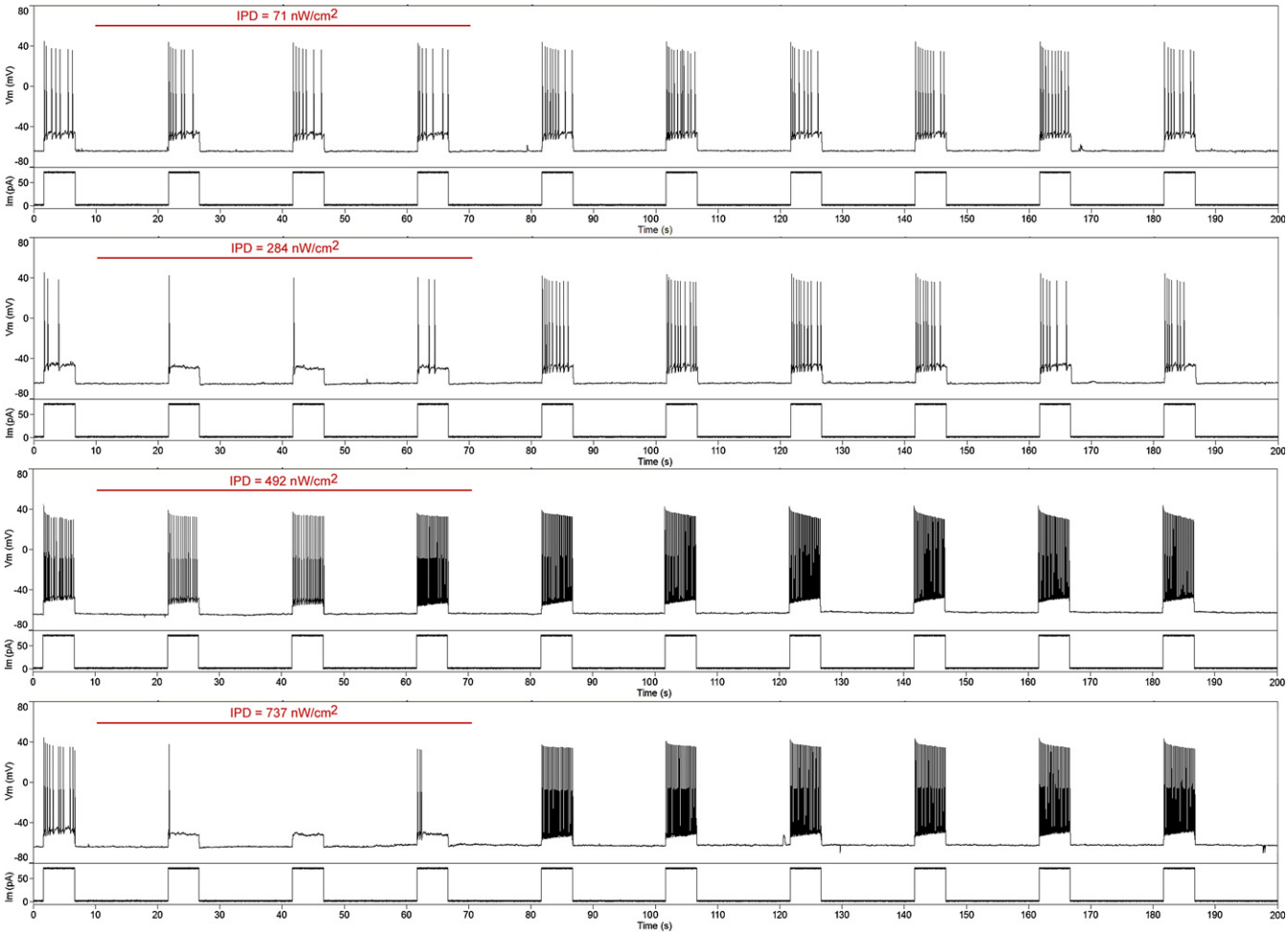

Figure 2. Sample recordings of neuronal activity in neuron n14 selected to show four IPD levels of MMW exposure, applied in random order during the experiment. For each record, two traces are shown: the top trace shows the intracellular voltage and the bottom shows the injected current. Red bars indicate the duration of the MMW exposure with the value above the bar indicating the IPD level.

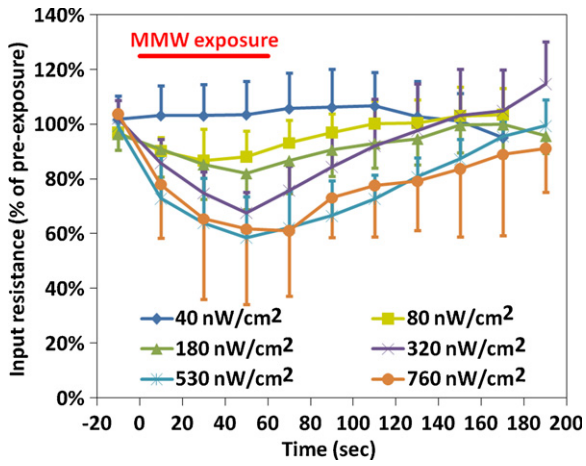

Figure 3. Latency of the MMW-induced suppression in R_n at different IPD levels. The red bar indicates the duration of the MMW exposure and values in the graph legend indicate the IPD levels. Error bars indicate the standard deviations.

exposures for different neurons were grouped into six levels, and the R_n values for these levels were averaged across the neurons for each time point (figure 3). Maximal R_n drop was evident at 50 s into the MMW exposure. Thus, the detailed evaluation of MMW effects on the neuronal activity and plasma membrane parameters in subsequent figures 4–8 and tables 1 and 2 was done using the values at 50 s into the exposure. After the exposure, the R_n values exhibited a gradual recovery, which was complete (or nearly complete for the highest IPD) after about 2 min. Following each exposure trial, we have allowed at least 3 min before commencing the next exposure to provide sufficient time to assure the recovery of baseline neuronal activity.

The firing rate and the AP amplitude were somewhat variable across the 25–30 min of recording, as can be seen in figure 2 in the trial with IDP of 492 nW cm^{-2}. In order to reduce the confounding influence of this variability on the effects of MMWs, the overall baseline value of the firing rate and AP amplitude was calculated by averaging the values from the baseline periods prior to each MMW exposure trial. The data for individual exposure trials were then normalized using a ratio of the pre-exposure baseline value in that particular trial to the overall baseline value.

No normalization was used for the pre-exposure variability in firing rate and AP amplitude across the neurons. Instead, we decided to group the neurons based on their

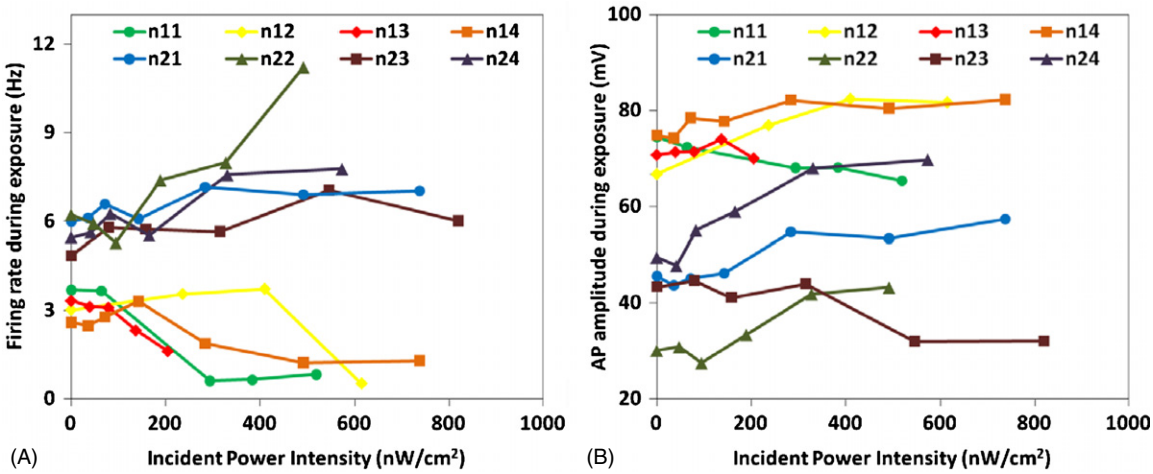

Figure 4. The effect of the IPD on the firing rate (A) and AP amplitude (B) in eight neurons.

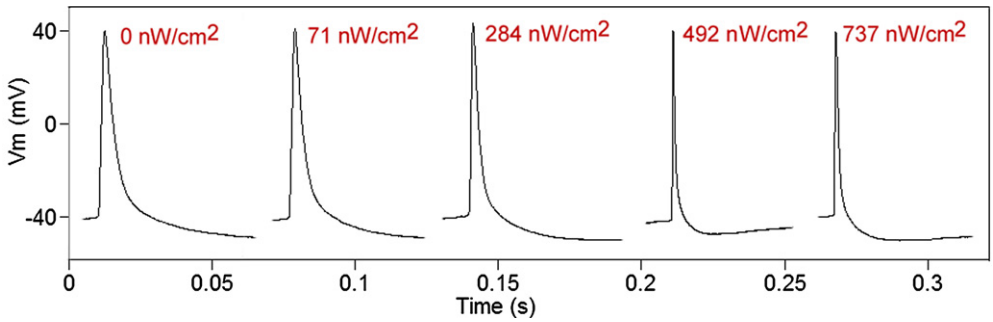

Figure 5. Sample AP profiles in neuron n14 before MMW exposure and at 50 s after the beginning of exposure at different IPD levels (indicated in red). In the experiment, these IPDs were applied in random order.

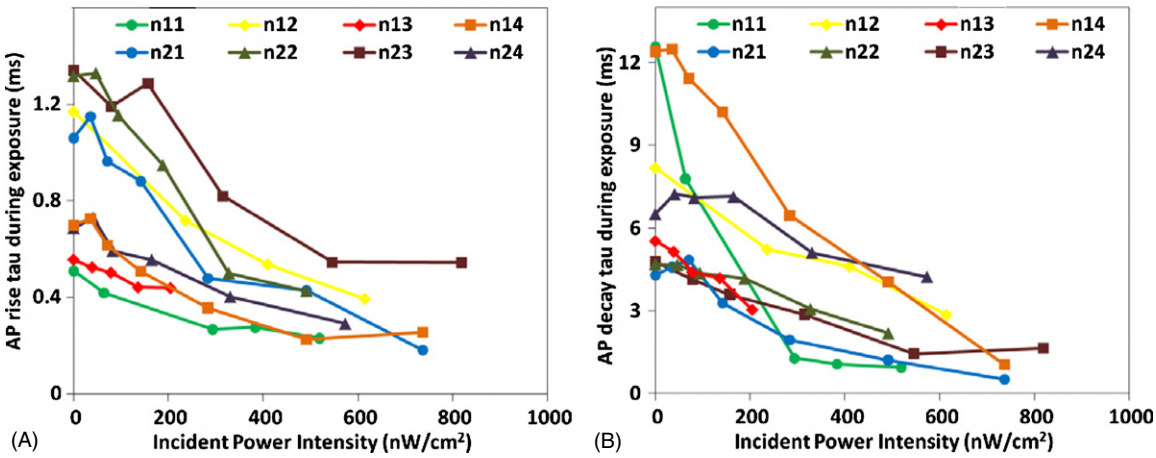

Figure 6. The effect of the IPD on τ_{rise} (A) and τ_{decay} (B) in eight neurons.

baseline firing rate. Two groups were identified: first ($n = 4$) with low (~3 Hz) and second ($n = 4$) with high (5–6 Hz) firing rate (figure 4 and table 1). The low-firing group exhibited strong suppression of neuronal firing by the MMWs, while the neurons in the second group exhibited either facilitation ($n = 2$) or remained relatively unchanged (figure 4(A)). The neurons in the first group also exhibited higher baseline AP amplitudes (~70 mV) as compared to the second group (30–50 mV). Low baseline AP amplitude in the neuron n22 can be potentially attributed to uncompensated capacitance in the electrode. In both groups, there appeared to be a small (if any) effect of the MMWs on the AP amplitude even at the highest IDP levels.

To examine the possible changes in the plasma membrane characteristics, we examined the shape of the individual APs and the input resistance of the membrane. The profiles of APs were compared prior to MMW exposure and at 50 s during the MMW exposure at several IPD levels (figure 5). Noticeable narrowing of the peaks can be readily observed at higher IPD levels. This narrowing was completely reversed

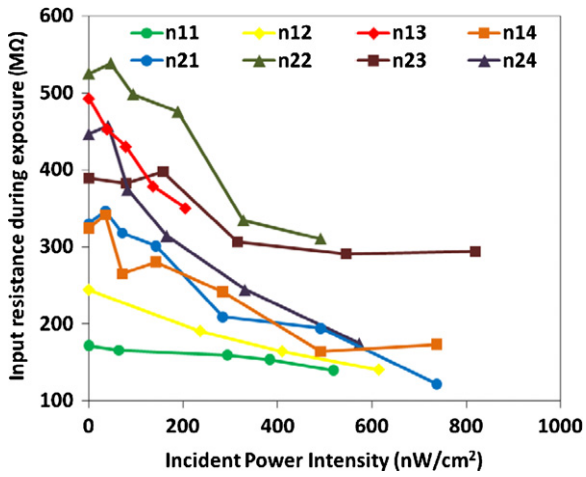

Figure 7. The effect of the IPD on R_n in eight neurons.

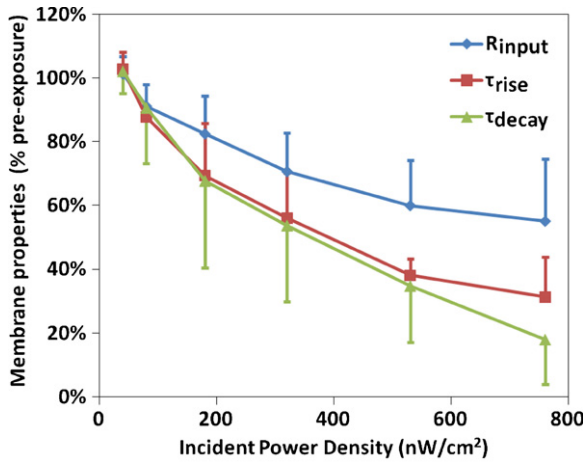

Figure 8. Relative reduction in R_n τ_{rise} and τ_{decay} as a function of the MMW IPD, averaged from eight neurons.

to the baseline level within 2 min after the exposure (data not shown).

Quantification of the time constants for the AP rise and decay phases (τ_{rise} and τ_{decay}) confirmed the remarkable decrease in both parameters proportional to the increasing strength of IPD and this effect was clearly dose dependent on the level of IDP (figure 6).

R_n was markedly affected by the MMW exposure. The R_n drop, similar to the peak narrowing, was strongly IPD dose dependent, and in most neurons at high IPDs, the R_n value dropped below 200 MΩ (figure 7).

Out of the eight neurons studied, two neurons (n13 and n14) were examined in the absence of intracellular calcium signaling, accomplished by buffering the intracellular Ca^{2+} stores with 10 mM EGTA, added to the pipette solution. As evident from figures 4, 6, and 7, there was no apparent difference in the responses of these neurons (n13 and n14) as compared to other neurons in this study. Their baseline values and MMW-induced changes in the τ_{rise}, τ_{decay} and R_n values were indistinguishable from the others, and their firing rates and AP amplitudes were close to those of the non-Ca^{2+}-buffered neurons in group 1, n11 and n12.

Statistical evaluation of AP-related and membrane characteristics of two identified neuronal groups is presented in table 1. In group 1, MMW exposure reduced the firing rate to one third of the pre-exposure value, while in group 2 it was slightly increased. The AP amplitude in group 1 is increased by 14%, while in group 2 it remained unchanged. Both groups of neurons exhibited similar shortening of the rise and decay times of the AP peak and similar reduction of R_n.

Both groups of neurons exhibited similar reduction in their plasma membrane properties (R_n, τ_{rise}, and τ_{decay}): therefore, the data from all neurons were combined to evaluate their relative reduction as the function of MMW IPD (figure 8). These membrane properties, which are inversely correlated with the membrane conductivity, were dose-dependently reduced. At the highest IPD level, R_n was suppressed by more than 40%, and τ_{rise} and τ_{decay} were suppressed by more than 60% from their pre-exposure values.

The neuronal changes during exposure at the two strongest IPD levels were compared with changes, observed during heating of the aCSF bath with an in-line fluid heater, as reported previously by others (Lee *et al* 2005). While the temperature rise of aCSF during MMW exposure at the two highest IPD levels was only 2.1 and 3.2 °C versus 10 °C during bath heating, the observed MMW-induced decreases in τ_{rise}, τ_{decay} and R_n were considerably more pronounced (table 2). Specifically, the MMW exposure caused an 83% decrease in the AP width and 46% decrease in R_n, while the 10 °C bath heating produced only a 41% decrease in the AP width and a 35% decrease in R_n.

4. Discussion

This study provides the first real-time examination of single neuronal activity during MMW exposure in a slice preparation. The key findings in this study are the MMW-induced fully reversible effects on neuronal firing, the shape of the APs and R_n. These short-lasting effects were observed at extremely low IPD levels ($<1\ \mu\text{W cm}^{-2}$) of MMW and are stronger than those induced by 10 °C bath heating.

The observed MMW effects on the neuronal firing might be neuron subtype specific. A subset of layer 2/3 cortical neurons with low firing rate (group 1) has been most susceptible to suppression of neuronal firing by the applied MMWs, with a reduction to one third of the pre-exposure level. This dichotomy of responses might indicate the presence of different subtypes of pyramidal cells. Further studies with blockage of synaptic activity might be able to clarify the existence of such pyramidal neuron subpopulations and the mechanisms of their MMW-induced suppression of neuronal firing.

While the AP amplitude was not significantly affected by the MMW exposure, other AP parameters, τ_{rise} and τ_{decay} were strongly affected by the MMWs, with the total AP duration reduced from 8.3 to 1.4 ms (83% decrease) for the highest IPD level. A key characteristic of the membrane conductivity, R_n, was similarly dose-dependently reduced by

increasing IPD levels, indicating the channel opening. The coincident decrease in R_n, τ_{rise} and τ_{decay} is not surprising, as the narrowing of AP spikes is strongly correlated with decreased R_n (Trevelyan and Jack 2002). The 10 °C bath heating of cortical neurons has a negligible effect on the AP amplitude and significantly reduces R_n, τ_{rise} and τ_{decay} (Lee *et al* 2005).

If MMW action on the neurons is largely thermal, then some of the same mechanisms implicated in the effects of heating might be involved. One such proposed mechanism for the heating-dependent changes in the neuronal membrane properties involves a temperature-dependent increase in K^+ channel function (presumably due to faster channel activation), while Na^{2+} channel function remains relatively constant (Volgushev *et al* 2000b, Cao and Oertel 2005). A modeling study of R_n in the cortical pyramidal neurons also indicated an important role of the increased membrane conductance in the thermally induced effects (Trevelyan and Jack 2002). The MMWs effects in this study were considerably stronger than those evoked by 10 °C bath heating, while the temperature rise at two highest IPD levels reached only 2.1 and 3.2 °C. It may be possible that some of the MMW-induced effects in this study were mediated through non-thermal mechanisms, involving specific absorption of the MMWs by neural tissue. Specific absorption of MMWs by plasma membrane-bound water, phospholipids and other dipole-oriented molecules has previously been demonstrated (Enders and Nimtz 1984, Liburdy and Magin 1985, Cametti *et al* 1988, Beneduci 2008, Ramundo-Orlando *et al* 2009). The involvement of specific plasma membrane ion channels in the non-thermal mechanism of MMW action remains to be explored.

In an attempt to differentiate the direct effects of MMWs on the voltage-sensitive channels in the plasma membrane from possible indirect activation of the membrane-bound ion channels through intracellular second messenger-mediated signaling, we blocked the intracellular Ca^{2+}-dependent second messenger signaling in two neurons. This was accomplished using a pipette solution with a calcium chelator (10 mM EGTA), which buffers the intracellular calcium stores and thus eliminates the possible effect of intracellular calcium fluctuations on the membrane potential (Maravall *et al* 2000, Harks *et al* 2003). The obtained results suggest that Ca^{2+}-dependent second messenger signaling does not significantly affect the induced changes in the AP generation and plasma membrane properties, implying the importance of direct voltage-sensitive channel opening for mediating the MMW effects.

In summary, the key finding of this study is the demonstration that low levels of MMW power can induce changes in neuronal firing and a profound reduction of R_n, which in turn may lead to increased neuronal excitability (Volgushev *et al* 2000a). In this study, neurons were effectively inhibited at a depth of 2 mm under the aCSF, but it remains to be seen whether the MMWs can produce similar changes in neuronal activity when applied in the human skin and/or central nervous system. More studies are needed to evaluate the possibility of inducing long-term changes in the neuronal excitability by MMWs in order to establish the feasibility of using MMW for therapeutic neuromodulation.

Acknowledgments

The authors would like to acknowledge administrative and technical support from Professor David B Rutledge, California Institute of Technology, and financial support from the Huntington Medical Research Institutes and the Chief Scientist's Office of the Jet Propulsion Laboratory. Helpful suggestions from the anonymous reviewers are also gratefully acknowledged.

References

Alekseev S I, Gordiienko O V, Radzievsky A A and Ziskin M C 2010 Millimeter wave effects on electrical responses of the sural nerve *in vivo Bioelectromagnetics* **31** 180–90

Beneduci A 2008 Review on the mechanisms of interaction between millimeter waves and biological systems *Bioelectrochemistry Research Developments* ed E M Bernstein (New York: Nova Science Publishers) pp 35–80

Cametti C, De Luca F, Macri M A, Maraviglia B and Sorio P 1988 Audio to microwave frequency dielectric study of the pretransition region in DPL-water systems *Liq. Cryst.* **3** 839–45

Cao X-J and Oertel D 2005 Temperature affects voltage-sensitive conductances differentially in octopus cells of the mammalian cochlear nucleus *J. Neurophysiol.* **94** 821–32

Chou C-K and D'Andrea J (ed) 2006 *IEEE Standard for Safety Levels with Respect to Human Exposure to Radio Frequency Electromagnetic Fields, 3 kHz to 300 GHz*

Enders A and Nimtz G 1984 Dielectric relaxation study of dynamic properties of hydrated phospholipid bilayers *Ber. Bunsenges. Phys. Chem.* **88** 512–7

Harks E G A, Torres J J, Cornelisse L N, Ypey D L and Theuvenet A P R 2003 Ionic basis for excitability of normal rat kidney (NRK) fibroblasts *J. Cell. Physiol.* **196** 493–503

Hillert L, Åkerstedt T, Lowden A, Wiholm C, Kuster N, Ebert S, Boutry C, Moffat S D, Berg M and Arnetz B B 2008 The effects of 884 MHz GSM wireless communication signals on headache and other symptoms: an experimental provocation study *Bioelectromagnetics* **29** 185–96

Lawton G 2008 Wireless HD video heats up *Computer* **41** 18–20

Lee J C F, Callaway J C and Foehring R C 2005 Effects of temperature on calcium transients and Ca^{2+}-dependent after hyperpolarizations in neocortical pyramidal neurons *J. Neurophysiol.* **93** 2012–20

LeVine S 2009 *The Active Denial System. A Revolutionary, Non-lethal Weapon for Today's Battlefield* (Washington, DC: National Defence University) pp 1–17

Liburdy R P and Magin R L 1985 Microwave-stimulated drug release from liposomes *Radiat. Res.* **103** 266–75

Maravall M, Mainen Z F, Sabatini B L and Svoboda K 2000 Estimating intracellular calcium concentrations and buffering without wavelength ratioing *Biophys. J.* **78** 2655–67

Pakhomov A G, Prol H K, Mathur S P, Akyel Y and Campbell C B 1997 Search for frequency-specific effects of millimeter-wave radiation on isolated nerve function *Bioelectromagnetics* **18** 324–34

Ramundo-Orlando A, Longo G, Cappelli M, Girasole M, Tarricone L, Beneduci A and Massa R 2009 The response of giant phospholipid vesicles to millimeter waves radiation *Biochem. Biophys. Acta* **1788** 1497–507

Trevelyan A J and Jack J 2002 Detailed passive cable models of layer 2/3 pyramidal cells in rat visual cortex at different temperatures *J. Physiol.* **539** 623–36

Volgushev M, Vidyasagar T R, Chistiakova M and Eysel U T 2000a Synaptic transmission in the neocortex during reversible cooling *Neuroscience* **98** 9–22

Volgushev M, Vidyasagar T R, Chistiakova M, Yousef T and Eysel U T 2000b Membrane properties and spike generation in rat visual cortical cells during reversible cooling *J. Physiol.* **522** Pt 1 59–76

Wells J, Kao C, Jansen E D, Konrad P and Mahadevan-Jansen A 2005a Application of infrared light for *in vivo* neural stimulation *J. Biomed. Opt.* **10** 64003

Wells J, Kao C, Mariappan K, Albea J, Jansen E D, Konrad P and Mahadevan-Jansen A 2005b Optical stimulation of neural tissue *in vivo Opt. Lett.* **30** 504–6

Wiholm C, Lowden A, Kuster N, Hillert L, Arnetz B B, Akerstedt T and Moffat S D 2009 Mobile phone exposure and spatial memory *Bioelectromagnetics* **30** 59–65

Zhadobov M, Sauleau R, Le Drean Y, Alekseev S I and Ziskin M C 2008 Numerical and experimental millimeter-wave dosimetry for *in vitro* experiments *IEEE Trans. Microwave. Theory Tech.* **56** 2998–3007